НАУЧНО-ТЕХНИЧЕСКИЙ ВЕСТНИК ИНФОРМАЦИОННЫХ ТЕХНОЛОГИЙ, МЕХАНИКИ И ОПТИКИ
сентябрь–октябрь 2025 Том 25 № 5 http://ntv.ifmo.ru/
SCIENTIFIC AND TECHNICAL JOURNAL OF INFORMATION TECHNOLOGIES, MECHANICS AND OPTICS
September–October 2025 Vol. 25 No 5 http://ntv.ifmo.ru/en/
ISSN 2226-1494 (print) ISSN 2500-0373 (online)

doi: 10.17586/2226-1494-2025-25-5-807-816

Optical spin currents in chiral optical fibers

Ilya A. Deriy[1]✉, Danil F. Kornovan[2], Mihail I. Petrov[3], Andrey A. Bogdanov[4]

[1,4] Harbin Engineering University, Qingdao, 266000, China
[1,2,3,4] ITMO University, Saint Petersburg, 197101, Russian Federation

[1] ilya.deriy@metalab.ifmo.ru✉, https://orcid.org/0000-0002-6515-9325
[2] d.kornovan@metalab.ifmo.ru, https://orcid.org/0000-0002-4851-0697
[3] m.petrov@metalab.ifmo.ru, https://orcid.org/0000-0001-8155-9778
[4] a.bogdanov@metalab.ifmo.ru, https://orcid.org/0000-0002-8215-0445

Abstract
This paper is devoted to the study of optical chiral cylindrical waveguides from the point of view of their application in optical spintronics. In the paper, it is proposed to use a chiral optical cylindrical waveguide as an optical spin diode. The mode structure of the waveguide under consideration is calculated and the dispersion equation for fundamental modes of the waveguide with an azimuthal number $m = \pm 1$ is numerically solved for various values of the chirality parameter of the waveguide material. Expressions for the energy flux and the optical spin current inside the waveguide are derived. It is shown that in the single-mode regime, the direction of the optical spin currents in the waveguide is determined exclusively by the sign of the chirality parameter of the waveguide material, regardless of the azimuthal number and the direction of mode propagation. Due to this, the superposition of $m = 1$ and $m = -1$ modes propagating in opposite directions will have a zero energy flux, but a nonzero optical spin current. Our results expand the element base of optical spintronics and open up new ways for creating energy-efficient optical computing systems.

Keywords
optical spin, optical spintronics, chirality, optical information transfer, optical waveguides, optical nanofibers

Acknowledgements
The studies were supported by the Russian Science Foundation (Project 23-72-10059). Ilya Deriy acknowledges the BASIS Foundation for valuable support.

For citation: Deriy I.A., Kornovan D.F., Petrov M.I., Bogdanov A.A. Optical spin currents in chiral optical fibers. *Scientific and Technical Journal of Information Technologies, Mechanics and Optics*, 2025, vol. 25, no. 5, pp. 807–816. doi: 10.17586/2226-1494-2025-25-5-807-816

УДК 535.131

Оптические спиновые токи в хиральных оптоволокнах

Илья Александрович Дерий[1]✉, Данил Феодосьевич Корнован[2], Михаил Игоревич Петров[3], Андрей Андреевич Богданов[4]

[1,4] Харбинский Инженерный Университет, Циндао, 266000, Китай
[1,2,3,4] Университет ИТМО, Санкт-Петербург, 197101, Российская Федерация

[1] ilya.deriy@metalab.ifmo.ru✉, https://orcid.org/0000-0002-6515-9325
[2] d.kornovan@metalab.ifmo.ru, https://orcid.org/0000-0002-4851-0697
[3] m.petrov@metalab.ifmo.ru, https://orcid.org/0000-0001-8155-9778
[4] a.bogdanov@metalab.ifmo.ru, https://orcid.org/0000-0002-8215-0445

Аннотация
Представлено исследование оптических хиральных цилиндрических волноводов с точки зрения их применения в оптической спинтронике. Предложено использование хирального оптического цилиндрического волновода в роли оптического спинового диода. Рассчитана модовая структура рассматриваемого волновода и численно решено дисперсионное уравнение для фундаментальных мод волновода с азимутальным числом $m = \pm 1$ для

различных значений параметра хиральности материала волновода. Получены выражения для потока энергии и оптического спинового тока внутри волновода. Показано, что в одномодовом режиме работы волновода, направление протекания оптических спиновых токов в волноводе определяется исключительно знаком параметра хиральности материала волновода, вне зависимости от азимутального числа и направления распространения моды. Следовательно, суперпозиция $m = 1$ и $m = -1$ мод, распространяющихся в разных направлениях, будет иметь нулевой поток энергии, но ненулевой оптический спиновой ток. Полученные результаты расширяют элементную базу оптической спинтроники и открывают новые пути для создания энергоэффективных оптических вычислительных систем.

Ключевые слова
оптический спин, оптическая спинтроника, хиральность, оптические методы переноса информации, оптические волноводы, оптоволокно

Благодарности
Исследования поддержаны Российским научным фондом (проект 23-72-10059). Илья Дерий выражает благодарность Фонду развития теоретической физики и математики «БАЗИС» за неоценимую поддержку.

Ссылка для цитирования: Дерий И.А., Корнован Д.Ф., Петров М.И., Богданов А.А. Оптические спиновые токи в хиральных оптоволокнах // Научно-технический вестник информационных технологий, механики и оптики. 2025. Т. 25, № 5. С. 807–816 (на англ. яз.). doi: 10.17586/2226-1494-2025-25-5-807-816

Introduction

Photonics has rapidly advanced as a transformative technology providing numerous benefits compared to conventional electronics, including lower material losses, enhanced bandwidth capabilities, and significantly faster data transmission [1, 2]. While traditional electronic systems depend on the movement of electrons, photonics leverages the intrinsic characteristics of photons, notably their extremely high propagation speed and negligible mass. This intrinsic advantage ensures that photonic devices operate with substantially lower heat generation, resulting in higher operational frequencies and markedly improved energy efficiency relative to electronic devices [3–5]. However, the operation principle of most photonic and optoelectronic devices is based on electromagnetic energy which introduces severe difficulties into the engineering process of nonreciprocal and nonlinear optical devices, and imposes significant limitations on energy consumption and modulation frequencies.

Spintronics, similarly poised as a promising alternative to traditional electronics, utilizes the intrinsic spin of electrons rather than their charge for data storage and processing [6–8]. The utilization of spin degrees of freedom in electrons allows for energy-efficient data processing and storage, reduced heat generation, and increased device performance [9, 10]. Analogously, photons possess intrinsic angular momentum, comprised of Spin Angular Momentum (SAM), related to polarization, and Orbital Angular Momentum, arising from spatial phase distributions [11–13]. The manipulation of SAM and Orbital Angular Momentum of photons provides additional degrees of freedom for information encoding, transmission, and manipulation, enhancing the capabilities of optical communication systems and quantum computing technologies [14–16]. And recently it was shown that utilization of electromagnetic SAM as an information carrier allows for the implementation of the low-energy nonreciprocal optical devices such as optical diode and circulator without the violation of the Lorentz reciprocity [17]. However, the real-life implementation of an optical spin diode here was purely conceptual and far from real photonic systems.

Optical nanofibers have become particularly important in the field of photonics due to their exceptional ability to guide and confine light in extremely small volumes [18, 19]. These fibers are characterized by sub-wavelength diameters, enabling strong evanescent fields and efficient interaction between guided modes and surrounding materials or quantum emitters. Nanofibers offer significant advantages for applications in optical communications, sensing, and quantum information processing due to their high field intensity, low loss, flexibility, and ease of integration into existing photonic platforms [20, 21]. The convenience, versatility, and widespread availability of optical nanofibers have made them ubiquitous in modern photonic technologies.

In this work, we extend the ideas developed in [17] on the use of optical spin currents for optical communication and information processing. We show that a chiral optical nanofiber can operate in the optical spin diode regime. To confirm this fact, we solve the eigenstate problem for a chiral optical waveguide, derive expressions for the energy flux and the SAM flux in such a waveguide, and show that in the nanofiber regime, the electromagnetic energy can propagate in either direction, while the direction of propagation of the optical spin currents is strictly specified, and is determined by the sign of the chirality parameter of the waveguide material. We note that while all results presented in this paper are for chiral waveguides made of isotopic chiral materials, the same physics can be observed for structurally chiral waveguides, e.g. like in [22–24].

Eigenmodes of a Chiral Cylindrical Waveguide

Consider a cylindrical waveguide with radius a whose axis is directed along the z-axis (Fig. 1, a). The waveguide under consideration is made of an isotropic chiral material with permittivity ϵ, permeability $\mu = 1$, and chirality parameter χ. For simplicity, we consider air to be the surrounding medium. Following the default approach for the solution of an eigenmode problem for a cylindrical waveguide, we find eigenmodes by solving Maxwell's equations inside and outside of the waveguide, and then use boundary conditions to find unknown complex coefficients.

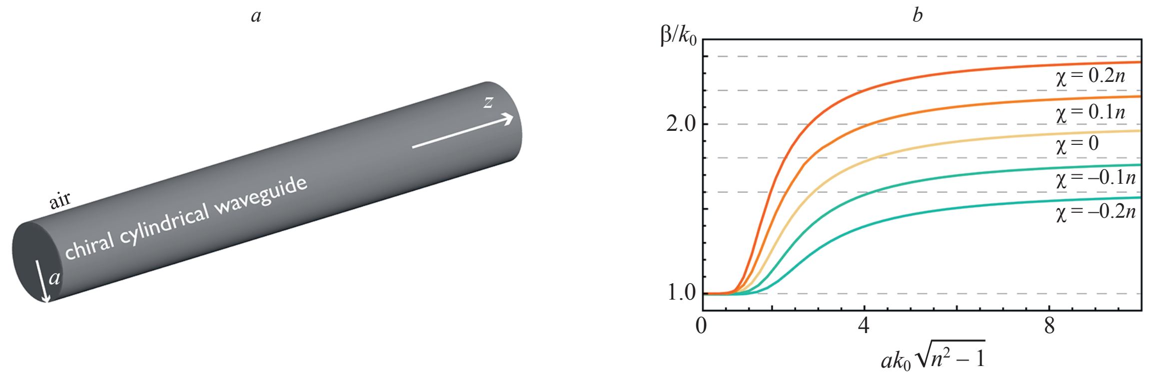

Fig. 1. Isotropic chiral waveguide. Geometry of the waveguide (*a*). Dispersion of the fundamental mode with azimuthal number $m = 1$ for the value of the refractive index $n = 2$, and different values of χ (*b*). Variables k_0 and β encode freespace wavenumber and propagation constant accordingly

In an arbitrary homogeneous chiral medium with material parameters ϵ, μ, and χ, in the basis of Riemann-Silberstein vectors (see section "Supplementary Materials"), Maxwell's equations can be written as

$$\nabla\times\mathbf{F}_\pm(\mathbf{r}) = \pm k_0 n_\pm \mathbf{F}_\pm(\mathbf{r}),\quad n_\pm = n \pm \chi, \tag{1}$$

where $\mathbf{F}_\pm(\mathbf{r}) = \mathbf{E}(\mathbf{r}) \pm i\sqrt{\mu/\epsilon}\,\mathbf{H}(\mathbf{r})$ are the Riemann-Silberstein vectors [25, 26]; $n = \sqrt{\epsilon\mu}$ is the refractive index of the media; $k_0 = \omega/c$ is the freespace wavenumber.

Riemann-Silberstein vectors separates electromagnetic fields into two physically independent chiral components with sign ± encoding the helicity of the field, which makes such a basis a very natural choice for the chiral materials. In addition, due to the cylindrical symmetry of the problem, we can use the following ansatz [27]

$$\mathbf{F}_\pm(\mathbf{r}) = \mathbf{F}_{\pm,m}(\rho, \beta)e^{im\varphi + i\beta z}, \tag{2}$$

where m is the angular momentum number; β is the propagation constant; ρ and φ are the radial and angular coordinates in the cylindrical system of coordinates.

Thus, in cylindrical coordinates, Eq. (1) can be written as (omitting index m and argument β for the sake of brevity)

$$\frac{im}{\rho}F_{\pm,z}(\rho) - i\beta F_{\pm,\varphi}(\rho) = \pm n_\pm k_0 F_{\pm,\rho}(\rho), \tag{3}$$

$$i\beta F_{\pm\rho}(\rho) - \partial_\rho F_{\pm,z}(\rho) = \pm n_\pm k_0 F_{\pm,\varphi}(\rho), \tag{4}$$

$$\frac{1}{\rho}[\partial_r(\rho F_{\pm\varphi}(\rho)) - imF_{\pm,\rho}(\rho)] = \pm n_\pm k_0 F_{\pm,z}(\rho), \tag{5}$$

from which it is possible to derive the following relations,

$$\begin{gathered}\left[\frac{\pm imn_\pm k_0}{\rho} + i\beta\partial_\rho\right]F_{\pm,z}(\rho) = \kappa_\pm^2 F_{\pm,\rho}(\rho),\\ \left[\frac{m\beta}{\rho} \mp n_\pm k_0\partial_\rho\right]F_{\pm,z}(\rho) = \kappa_\pm^2 F_{\pm,\varphi}(\rho),\end{gathered} \tag{6}$$

where $\kappa_\pm^2 = n_\pm^2 k_0^2 - \beta^2$, and the equation for $F_{\pm,z}$

$$\rho\partial_\rho[\rho\partial_\rho F_{\pm,z}(\rho)] + [\rho^2\kappa_\pm^2 - m^2]F_{\pm,z}(\rho) = 0. \tag{7}$$

Eq. (7) is the Bessel equation, which solution are Bessel functions. To satisfy the regularity condition for the solution at the origin $\rho = 0$, and to satisfy the outgoing boundary conditions, we choose a Bessel function of the first kind $J_m(\kappa_\pm^{\text{in}}\rho)$ for the fields inside the waveguide, and a Hankel function of the first kind $H_m^{(I)}(\kappa_\pm^{\text{out}}\rho)$ for the fields outside of the waveguide

$$\begin{gathered}F_{\pm,z}^{\text{in}}(\rho) = a_\pm \kappa_\pm^{\text{in}2} J_m(\kappa_\pm^{\text{in}}\rho),\\ F_{\pm,z}^{\text{out}}(\rho) = b_\pm \kappa_\pm^{\text{out}2}\rho H_m^{(1)}(\kappa_\pm^{\text{out}}\rho),\end{gathered} \tag{8}$$

where indices "in" and "out" encode fields inside and outside of the waveguide; $a_\pm$ and $b_\pm$ are the complex amplitudes yet to be determined.

To find complex amplitudes $a_\pm$ and $b_\pm$, we substitute the obtained solution into a set of boundary conditions, which reads as

$$\begin{gathered}F_{+,\tau}^{\text{in}}(a) + F_{-,\tau}^{\text{in}}(a) = F_{+,\tau}^{\text{out}}(a) + F_{-,\tau}^{\text{out}}(a),\\ \frac{F_{+,\tau}^{\text{in}}(a) - F_{-,\tau}^{\text{in}}(a)}{\sqrt{\mu^{\text{in}}/\epsilon^{\text{in}}}} = \frac{F_{+,\tau}^{\text{out}}(a) - F_{-,\tau}^{\text{out}}(a)}{\sqrt{\mu^{\text{out}}/\epsilon^{\text{out}}}}.\end{gathered} \tag{9}$$

where τ encodes tangential component of the vector field; $\mu^{\text{in/out}}$, $\epsilon^{\text{in/out}}$ are the permeability and permittivity of the material of the core (in) and claddings (out) of the waveguide.

Expressions for the angular component of the fields can be derived from Eqs. (6), and (8)

$$\begin{gathered}F_{\pm,\varphi}^{\text{in}}(\rho) = Q_{m,\pm}(\kappa_\pm^{\text{in}}\rho) =\\ = a_\pm\left[-\frac{m\beta}{\rho}J_m(\kappa_\pm^{\text{in}}\rho) \mp n_\pm^{\text{in}}\,\kappa_\pm^{\text{in}}\,k_0 J_m'(\kappa_\pm^{\text{in}}\rho)\right],\\ F_{\pm,\varphi}^{\text{out}}(\rho) = P_{m,\pm}(\kappa\rho) =\\ = b_\pm\left[-\frac{m\beta}{\rho}H_m(\kappa_\pm^{\text{out}}\rho) \mp n_\pm^{\text{out}}\,\kappa_\pm^{\text{out}}\,k_0 H_m'(\kappa_\pm^{\text{out}}\rho)\right].\end{gathered} \tag{10}$$

Combining Eqs. (8)–(10), and introducing dimensionless parameters

$$\begin{gathered}\tilde{\kappa}_\pm \equiv a\kappa_\pm^{\text{in}} = \sqrt{n_\pm^2\tilde{k}^2 - \tilde{\beta}^2},\ \tilde{\kappa} \equiv a\kappa_\pm^{\text{out}} = \sqrt{\tilde{k}^2 - \tilde{\beta}^2},\\ \tilde{k} = ak_0,\ \tilde{\beta} = a\beta,\end{gathered} \tag{11}$$

and recalling that

$$\epsilon^{\mathrm{in}} = \epsilon,\ \epsilon^{\mathrm{out}} = 1,\ \mu^{\mathrm{in}} = \mu^{\mathrm{out}} = 1,\ \chi^{\mathrm{out}} = 0, \tag{12}$$

boundary conditions become

$$\begin{aligned} &a_+\tilde{\kappa}_+^2 J_m(\tilde{\kappa}_+) + a_-\tilde{\kappa}_-^2 J_m(\tilde{\kappa}_-) = (b_+ + b_-)\tilde{\kappa}^2 H_m(\tilde{\kappa}),\\ &a_+\tilde{\kappa}_+^2 nJ_m(\tilde{\kappa}_+) - a_-\tilde{\kappa}_-^2 nJ_m(\tilde{\kappa}_-) = (b_+ - b_-)\tilde{\kappa}^2 H_m(\tilde{\kappa}),\\ &a_+Q_{m,+}(\tilde{\kappa}_+) + a_-Q_{m,-}(\tilde{\kappa}_-) = b_+P_{m,+}(\tilde{\kappa}) + b_-P_{m,-}(\tilde{\kappa}),\\ &a_+nQ_{m,+}(\tilde{\kappa}_+) - a_-nQ_{m,-}(\tilde{\kappa}_-) = b_+P_{m,+}(\tilde{\kappa}) - b_-P_{m,-}(\tilde{\kappa}), \end{aligned} \tag{13}$$

where $n = \sqrt{\epsilon^{\mathrm{in}}}$. The solvability condition $\det\hat{\mathcal{D}} = 0$ gives the dispersion equation for the eigenmodes of the system. These equations can be simplified if we notice that

$$\begin{aligned} &b_+P_{m,+}(\tilde{\kappa}) \pm b_-P_{m,-}(\tilde{\kappa}) =\\ &= b_+[-m\tilde{\beta}H_m(\tilde{\kappa}) - \tilde{k}\tilde{\kappa}H_m'(\tilde{\kappa})] \pm\\ &\pm b_-[-m\tilde{\beta}H_m(\tilde{\kappa}) + \tilde{k}\tilde{\kappa}H_m'(\tilde{\kappa})] =\\ &= -(b_+ \pm b_-)m\tilde{\beta}H_m(\tilde{\kappa}) - (b_+ \mp b_-)\tilde{k}\tilde{\kappa}H_m'(\tilde{\kappa}). \end{aligned} \tag{14}$$

Introducing

$$c_\pm = (b_+ \pm b_-)H_m(\tilde{\kappa}), \tag{15}$$

we rewrite the boundary conditions in a matrix form as

$$\underbrace{\begin{bmatrix} \tilde{\kappa}_+^2 J_m(\tilde{\kappa}_+) & \tilde{\kappa}_-^2 J_m(\tilde{\kappa}_-) & -H_m(\tilde{\kappa}) & 0\\ n\tilde{\kappa}_+^2 J_m(\tilde{\kappa}_+) & -n\tilde{\kappa}_-^2 J_m(\tilde{\kappa}_-) & 0 & -H_m(\tilde{\kappa})\\ Q_{m,+}(\tilde{\kappa}_+) & Q_{m,-}(\tilde{\kappa}_-) & m\tilde{\beta}H_m(\tilde{\kappa}) & \tilde{k}\tilde{\kappa}H_m'(\tilde{\kappa})\\ nQ_{m,+}(\tilde{\kappa}_+) & -nQ_{m,-}(\tilde{\kappa}_-) & \tilde{k}\tilde{\kappa}H_m'(\tilde{\kappa}) & m\tilde{\beta}H_m(\tilde{\kappa}) \end{bmatrix}}_{\hat{\mathcal{D}}} \times$$

$$\times \begin{bmatrix} a_+\\ a_-\\ c_+\\ c_- \end{bmatrix} = 0. \tag{16}$$

It is possible to show that

$$\begin{aligned} &(m, \beta) \to (-m, -\beta) \Rightarrow (F_{\pm,\rho}, F_{\pm,\varphi}, F_{\pm,z}) \to\\ &\to (-1)^m(-F_{\pm,\rho}, -F_{\pm,\varphi}, F_{\pm,z}), \end{aligned} \tag{17}$$

which follows from Eqs. (6), (8), and expressions for the Bessel and Hankel functions of the negative order $J_{-m}(z) = (-1)^m J_m(z)$, $H_{-m}(z) = (-1)^m H_m(z)$. In addition,

$$\begin{aligned} &(m, \chi) \to (-m, -\chi) \Rightarrow (-1)^m(F_{\pm,\rho}, F_{\pm,\varphi}, F_{\pm,z}) \to\\ &\to (F_{\mp,\rho}, -F_{\mp,\varphi}, F_{\mp,z}). \end{aligned} \tag{18}$$

And, from Eqs. (17), and (18) it follows that

$$\begin{aligned} &(\beta, \chi) \to (-\beta, -\chi) \Rightarrow (F_{\pm,\rho}, F_{\pm,\varphi}, F_{\pm,z}) \to\\ &\to (-F_{\mp,\rho}, -F_{\mp,\varphi}, F_{\mp,z}). \end{aligned} \tag{19}$$

Symmetries in Eqs. (17)–(19) follow from the properties of the physical system, namely reciprocity, chirality, and time-reversibility. It is possible to show that each of the symmetries corresponds to the multiplication of $\hat{\mathcal{D}}$ rows/columns by a constant or to the row/column permutations. It is well-known that such transformations leave the determinant of the matrix invariant, and, as a consequence, lead to the corresponding degeneracies in the eigenmodes structure of the system.

By taking $\hat{\mathcal{D}} = 0$, we arrive at the dispersion equation which can be written as

$$2n\tilde{k}^2\tilde{\kappa}^2 H_m^2(\tilde{\kappa})J_m(\tilde{\kappa}_+)J_m(\tilde{\kappa}_-)\mathcal{F}_m(\tilde{k}, \tilde{\beta}, n, \chi) = 0, \tag{20}$$

where

$$\begin{aligned} \mathcal{F}_m(\tilde{k}, \tilde{\beta}, n, \chi) &= \tilde{\kappa}_+^2\tilde{\kappa}_-^2\mathcal{H}_m^2(\tilde{\kappa}) +\\ &+ \frac{\tilde{\kappa}(n^2+1)}{2n}\mathcal{H}_m(\tilde{\kappa})[4\tilde{k}\tilde{\beta}mn\chi - \tilde{\kappa}_+\tilde{\kappa}_-(n_+\tilde{\kappa}_-\mathcal{J}_m(\tilde{\kappa}_+))] +\\ &+ n_-\tilde{\kappa}_-\mathcal{J}_m(\tilde{\kappa}_-) + \left[n_+\tilde{\kappa}\tilde{\kappa}_+\mathcal{J}_m(\tilde{\kappa}_+) - \frac{\tilde{k}\tilde{\beta}(n_+^2-1)}{\tilde{\kappa}}\right] \times\\ &\times \left[n_-\tilde{\kappa}\tilde{\kappa}_-\mathcal{J}_m(\tilde{\kappa}_-) + \frac{\tilde{k}\tilde{\beta}(n_-^2-1)}{\tilde{\kappa}}\right], \end{aligned} \tag{21}$$

where

$$\mathcal{H}_m(x) = \frac{H_m'(x)}{H_m(x)},\ \mathcal{J}_m(x) = \frac{J_m'(x)}{J_m(x)}. \tag{22}$$

We note that for waveguide modes, $\tilde{\kappa}^2 < 0$, which corresponds to the total internal reflection regime. In this case, in the waveguide cladding, fields become evanescent instead of propagating. Mathematically, this means that a more natural choice for the fields outside of the waveguide is the modified Bessel function (Macdonald function). The conversion from the Hankel to the Macdonald function can be done via the introduction of the parameter ζ as

$$\tilde{\zeta} = \sqrt{\tilde{\beta}^2 - \tilde{\kappa}_0^2} \in \mathbb{R},\ \tilde{\kappa} = i\tilde{\zeta}. \tag{23}$$

Then, the Hankel functions will be expressed in terms of the modified Bessel functions as

$$H_m(\tilde{\kappa}) = \frac{2}{\pi i^{m+1}}K_m(\tilde{\zeta}),\ H_m'(\tilde{\kappa}) = \frac{2}{\pi i^{m+2}}K_m'(\tilde{\zeta}), \tag{24}$$

$$\mathcal{H}_m(\tilde{\kappa}) = -i\frac{K_m'(\tilde{\zeta})}{K_m(\tilde{\zeta})} \equiv -i\mathcal{K}_m(\tilde{\zeta}). \tag{25}$$

Eq. (20) is a quadratic equation for $\mathcal{H}_m$, thus it has two solutions, corresponding to EH and HE modes, as in the dielectric waveguide. We note that due to the presence of the reciprocity and time-reversal symmetry, the dispersion equation is invariant under each of the following transformations

$$\begin{aligned} &(\chi, \beta) \to (-\chi, -\beta),\ (m, \beta) \to (-m, -\beta),\\ &(m, \chi) \to (-m, -\chi). \end{aligned} \tag{26}$$

Dispersion in terms of the effective refractive index $n_{\mathrm{eff}} = \beta/k_0$ and size parameter $V = ak_0\sqrt{n^2 - 1}$ for the fundamental mode ($m = \pm 1$), calculated from Eq. (20), is presented in Fig. 1, *b* for $n = 2$ and different values of χ. The dispersion is plotted only for $m = 1$ and $\beta > 0$, however all other cases can be obtained from the symmetrical considerations. One can see that the dispersion of the fundamental mode for $\chi \neq 0$ is similar to the dispersion of a dielectric waveguide with dielectric permittivity $\epsilon = n_{\mp}^2$. Dispersion curves for the chiral waveguide have similar behavior to the dispersion curves for the dielectric waveguide. Namely, the effective refractive index of the fundamental waveguide mode with $m = 1$ lies in the range $n_{\text{eff}} \in [n_0, n_+]$, where $n_0 = 1$ is the refractive index of the waveguide cladding. This fact suggests that one can treat κ_+ as the transversal quasi-wavevector component of the mode, similar to the $\sqrt{n_{\text{in}}^2 k_0^2 - \beta^2}$ in the dielectric waveguides. From the symmetry of the system, one can show that the dispersion of the fundamental mode with $m = -1$ is the same as for the fundamental mode with $m = 1$, but for the chirality parameter equal to $-\chi$. In particular, the effective refractive index of the mode with $m = -1$ will lie in the range $n_{\text{eff}} \in [n_0, n_-]$, and the transversal quasi-wavevector component will be κ_-. Fig. 2 shows the dependence of the effective refractive index of the fundamental eigenmodes (with $m = \pm 1$) on the chirality parameter in the different regions of the dispersion curve. Near the cutoff ($ak_0\sqrt{\epsilon - 1} = 1.01$, Fig. 2, *a*), the effective refractive index shows nonlinear dependence on the chirality parameter, however the difference $\Delta n_{\text{eff}} = n_{\text{eff}}(\chi) - n_{\text{eff}}(-\chi)$ is negligible. Far from cut-off, as expected, the behaviour of the effective refractive index is close to a straight line $n_{\text{eff}} \approx n_{\pm}$.

Power and SAM Flow

Energy flow and optical SAM flow inside the waveguide can be calculated as (see section "Supplementary Materials")

$$\langle P_z^{\text{in}} \rangle = \langle P_{z,+}^{\text{in}} \rangle + \langle P_{z,-}^{\text{in}} \rangle, \ \langle J_{zz}^{\text{in}} \rangle = \langle J_{zz,+}^{\text{in}} \rangle + \langle J_{zz,-}^{\text{in}} \rangle, \quad (27)$$

where

$$\langle P_{z,\pm}^{\text{in}} \rangle = \mp \frac{cn}{8} \int_0^a \text{Im}\{F_{\pm,\rho}^{\text{in}}(\rho) F_{\pm,\varphi}^{\text{in}*}(\rho)\} \rho \, d\rho, \quad (28)$$

and

$$\langle J_{zz,+}^{\text{in}} \rangle = \pm \frac{cn}{32k_0} \int_0^a \left[|F_{\pm,\rho}^{\text{in}}(\rho)|^2 + |F_{\pm,\varphi}^{\text{in}}(\rho)|^2 - |F_{\pm,z}^{\text{in}}(\rho)|^2 \right] \rho \, d\rho. \quad (29)$$

Each of the integrals above can be presented in the following form

$$I = c_1 \int_0^a \frac{J_m^2(\kappa\rho)}{\rho} d\rho + c_2 \int_0^a J_m(\kappa\rho) J_m'(\kappa\rho) \, d\rho + c_3 \int_0^a J_m'^2(\kappa\rho) \rho \, d\rho + c_4 \int_0^a J_m^2(\kappa\rho) \rho \, d\rho. \quad (30)$$

We note that all the integrals above are calculated for the case of $m \geq 0$, however, since $J_{-m}(x) = (-1)^m J_m(x)$ and $H_{-m}(x) = (-1)^m H_m(x)$, all quadratic forms of Bessel functions of same m will be invariant under the transformation $m \to -m$. The integral

$$I_4 = \int_0^a J_m^2(\kappa\rho) \rho \, d\rho = \frac{a^2}{2} [J_m^2(a\kappa) - J_{m-1}(a\kappa) J_{m+1}(a\kappa)] \quad (31)$$

can be easily evaluated using the Lommel's integral. The integral

$$I_2 = \int_0^a J_m(\kappa\rho) J_m'(\kappa\rho) \, d\rho = \frac{1}{\kappa} \int_0^{\kappa a} J_m(x) \frac{dJ_m(x)}{dx} dx = \frac{J_m^2(a\kappa) - J_m^2(0)}{\kappa}, \quad (32)$$

is straightforward. Integrals

$$I_1 = \int_0^a \frac{J_m^2(\kappa\rho)}{\rho} d\rho = \frac{(a\kappa)^{2m}}{4^m} \Gamma(2m) {}_2\tilde{F}_3(m, \frac{1}{2} + m; 1 + m, 1 + m, 1 + 2m; -a^2\kappa^2), \quad (33)$$

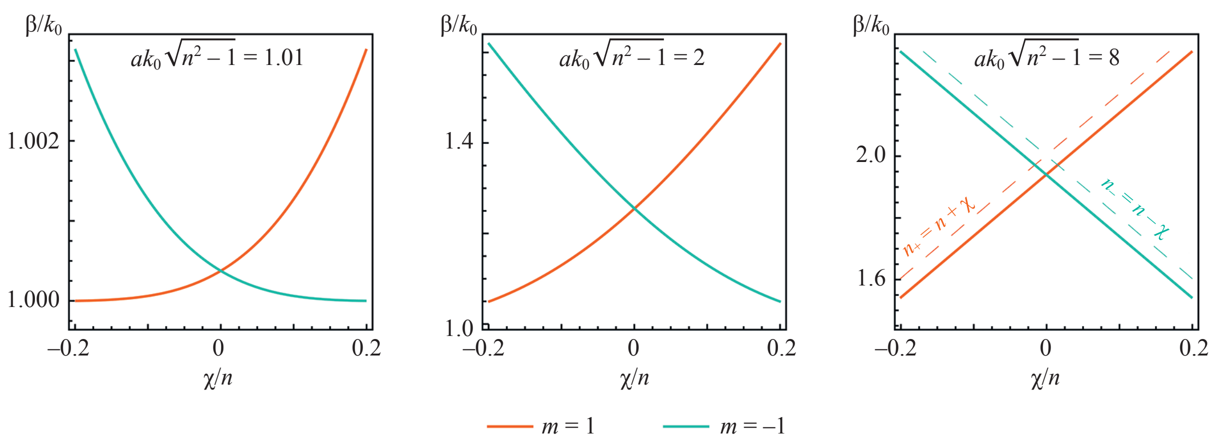

Fig. 2. Dependence of the effective refractive index $n_{\text{eff}} = \beta/k_0$ of the fundamental eigenmodes of the waveguide ($m = \pm 1$) vs. the normalized chirality parameter χ/n for different values of the dimensionless size parameter $V = ak_0\sqrt{\epsilon - 1} = 1.01$ (*a*); $V = 2$ (*b*); $V = 8$ (*c*)

where $\Gamma(x)$ is the Gamma function, and

$$I_3 = \int_0^a J'^2_m(\kappa\rho)\rho\, d\rho = \frac{1}{4}\int_0^a [J^2_{m-1}(\kappa\rho) + J^2_{m+1}(\kappa\rho) - 2J_{m-1}(\kappa\rho)J_{m+1}(\kappa\rho)]\rho\, d\rho = \frac{a^2}{8}[J^2_{m-1}(a\kappa) - J_{m-2}(a\kappa)J_m(a\kappa)] + \frac{a^2}{8}[J^2_{m+1}(a\kappa) - J_m(a\kappa)J_{m+2}(a\kappa)] + \frac{a^2(a\kappa)^{2m} m\, m!}{2^{2m+1}}\Gamma(2m)\,{}_3\tilde{F}_4\left(\frac{1}{2} + m, 1 + m, 1 + m; m, 2 + m, 2 + m, 1 + 2m; -a^2\kappa^2\right), \tag{34}$$

can be evaluated with the help of the regularized hypergeometric function ${}_p\tilde{F}_q$ [28]. Finally,

$$\langle P^{\rm in}_{z,\pm}\rangle = \mp |a_\pm|^2 \frac{cn}{8} \operatorname{Im}\{\mp i m^2 n_\pm k_0 \beta I_1 - im\kappa_\pm(\beta^2 + n^2_\pm k_0^2)I_2 \mp i\beta n_\pm k_0 \kappa^2_\pm I_3\} = \frac{cn}{8}[n_\pm k_0\beta(m^2 I_1 + \kappa^2_\pm I_3) \pm (\beta^2 + n^2_\pm k^2_0)\kappa_\pm I_2], \tag{35}$$

$$\langle J^{\rm in}_{zz,+}\rangle = \pm |a_\pm|^2 \frac{cn}{32k_0}[m^2(n^2_\pm k^2_0 + \beta^2)I_1 \pm 4mn_\pm k_0\beta\kappa_\pm I_2 + \kappa^2_\pm(n^2_\pm k^2_0 + \beta^2)I_3 - \kappa^4_\pm I_4] = \pm |a_\pm|^2 \frac{cn}{32k_0}[(n^2_\pm k^2_0 + \beta^2)(m^2 I_1 + \kappa^2_\pm I_3) \pm 4mn_\pm k_0\beta\kappa_\pm I_2 - \kappa^4_\pm I_4]. \tag{36}$$

For the fundamental mode with $m \pm 1$,

$$I_1 = \frac{1 - J^2_0(a\kappa) - J^2_1(a\kappa)}{2},\quad \kappa I_2 = J^2_1(a\kappa),$$
$$\kappa^2 I_3 = \frac{-1 + (a^2\kappa^2 + 1)J^2_0(a\kappa) + (a^2\kappa^2 - 1)J^2_1(a\kappa)}{2}, \tag{37}$$
$$\kappa^2 I_4 = \frac{a^2\kappa^2}{2}[J^2_1(a\kappa) - J_0(a\kappa)J_2(a\kappa)],$$

and

$$m^2 I_1 + \kappa^2 I_3 = \frac{a^2\kappa^2 J^2_0(a\kappa) + (\kappa^2 - 2)J^2_1(a\kappa)}{2}. \tag{38}$$

Thus, for the fundamental mode

$$\langle P^{\rm in}_{z,\pm}\rangle = |a_\pm|^2 \frac{cn}{8a^2}\left[\frac{n_\pm \tilde{k}_0\tilde{\beta}}{2}[\tilde{\kappa}^2_\pm J^2_0(\tilde{\kappa}_\pm) + (\kappa^2_\pm - 2)J^2_1(\tilde{\kappa}_\pm)] \pm (\tilde{\beta}^2 + n^2_\pm \tilde{k}^2_0)J^2_1(\tilde{\kappa}_\pm)\right], \tag{39}$$

$$\langle J^{\rm in}_{zz,+}\rangle = \pm |a_\pm|^2 \frac{cn}{32a^2k_0}\left[\frac{n^2_\pm\tilde{k}^2_0 + \tilde{\beta}^2}{2}[\tilde{\kappa}^2_\pm J^2_0(\tilde{\kappa}_\pm) + (\kappa^2_\pm - 2)J^2_1(\tilde{\kappa}_\pm)] \pm 4n_\pm\tilde{k}_0\tilde{\beta}J^2_1(\tilde{\kappa}_\pm) - \frac{\tilde{\kappa}^2_\pm}{2}[J^2_1(\tilde{\kappa}_\pm) - J_0(\tilde{\kappa}_\pm)J_2(\tilde{\kappa}_\pm)]\right]. \tag{40}$$

Optical spin diode regime

In the nanofiber regime, when $ak_0 << 1$, by doing a series expansion in ak and leaving only the leading terms, the eigenmode equation for $m = 1$ mode becomes

$$\begin{bmatrix} \frac{\tilde{\kappa}^3_+}{2} & \frac{\tilde{\kappa}^3_-}{2} & \frac{2\tilde{\kappa}}{\pi} & 0 \\ \frac{n\tilde{\kappa}^3_+}{2} & -\frac{n\tilde{\kappa}^3_-}{2} & 0 & \frac{2\tilde{\kappa}}{\pi} \\ -\tilde{\kappa}_+\frac{n_+\tilde{k} + \tilde{\beta}}{2} & \tilde{\kappa}_-\frac{n_-\tilde{k} - \tilde{\beta}}{2} & -\frac{2i\tilde{\beta}}{\pi\tilde{\kappa}} & \frac{2i\tilde{k}}{\pi\tilde{\kappa}} \\ -n\tilde{\kappa}_+\frac{n_+\tilde{k} + \tilde{\beta}}{2} & -n\tilde{\kappa}_-\frac{n_-\tilde{k} - \tilde{\beta}}{2} & \frac{2i\tilde{k}}{\pi\tilde{\kappa}} & -\frac{2i\tilde{\beta}}{\pi\tilde{\kappa}} \end{bmatrix} \begin{bmatrix} a_+ \\ a_- \\ c_+ \\ c_- \end{bmatrix} = 0, \tag{41}$$

with two solutions

$$a_+ = \frac{2i}{n\pi\tilde{\beta}},\ a_- = \frac{2i}{n\pi\tilde{\beta}},\ c_+ = 1,\ c_- = 0, \tag{42}$$

and

$$a_+ = \frac{2i}{n\pi\tilde{\beta}},\ a_- = -\frac{2i}{n\pi\tilde{\beta}},\ c_+ = 0,\ c_- = 1. \tag{43}$$

In addition, expressions for the energy and SAM flow became

$$\langle P^{\rm in}_{z,\pm}\rangle = |a_\pm|^2\, \tilde{\kappa}^2_\pm \frac{cn}{8a^2}\frac{n_\pm\tilde{k}_0\tilde{\beta}}{4},$$
$$\langle J^{\rm in}_{zz,\pm}\rangle = \pm |a_\pm|^2\, \tilde{\kappa}^2_\pm \frac{cn}{32a^2k_0}\frac{n^2_\pm\tilde{k}^2_0 + \tilde{\beta}^2}{4}. \tag{44}$$

Using Eqs. (42), and (43), and noting the fact that near the cutoff, $\beta \approx \eta k$, $\eta = \pm 1$, one can write that

$$\langle P^{\rm in}_z\rangle = \frac{c\eta}{4a^2\pi^2}(n^2 + 3\chi^2 - 1),$$
$$\langle J_{zz}\rangle = \frac{c\chi}{4a^2\pi^2 k_0}(n^2 + \chi^2). \tag{45}$$

Eqs. (45) are the key result of the paper. They show that the direction of the energy flow in the waveguide is governed by the direction of the propagation of the waveguide mode as in the traditional dielectric nanofibers. However, the direction of an optical spin current is governed by the sign of the chirality parameter.

From the orthogonality of the complex exponents $e^{im\varphi}$ and $e^{i\beta z}$ it follows that contribution of the different waveguide modes into the total energy and SAM flow is additive. In addition, it follows from Eq. (17) that transformation $(m, \beta) \to (-m, -\beta)$ leads to a transformation $\hat{\mathcal{D}} \to (-1)^m\hat{\mathcal{D}}$ since only φ and z components of the fields participate in the boundary conditions. Therefore, the eigenmode equation $\hat{\mathcal{D}}\mathbf{v} = 0$ is unchanged, which means

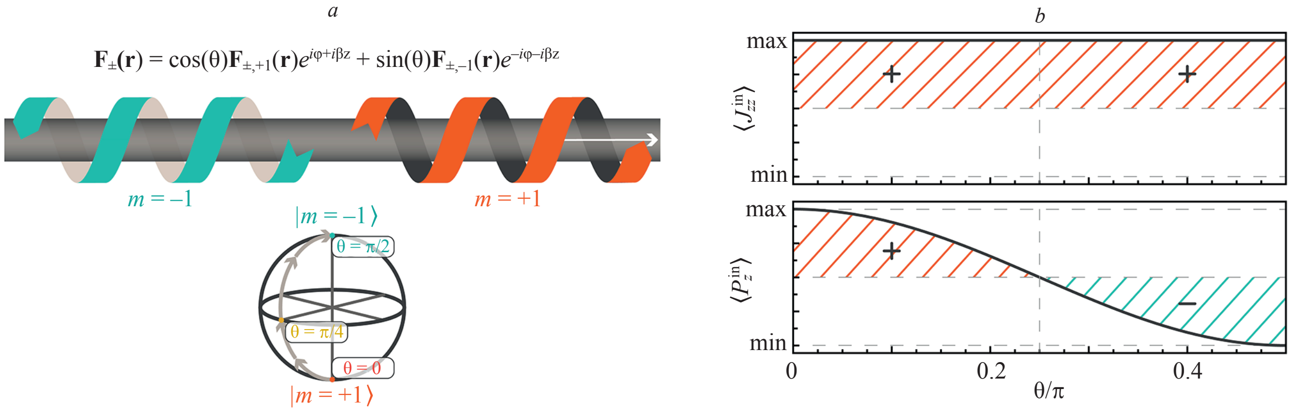

Fig. 3. Spin currents in an isotropic chiral nanofiber. Schematical representation of the propagation of the superposition of $m = 1$ and $m = -1$ modes in the optical spin diode regime (*a*). Spin Angular Momentum flux (spin current) and energy flux as a function of the parameter θ (*b*)

that both the eigenfrequencies and the eigenvectors of coefficients are identical for $m = 1$ and $m = -1$ eigenmodes.

This suggests that combination of two modes with opposite SAM (i.e. modes with $m = 1$ and $m = -1$) propagating in the opposite directions (Fig. 3, *a*) will lead to the emergence of the standing wave with zero energy transfer but nonzero optical spin current. Indeed, for a following configuration of fields

$$\mathbf{F}_{\pm}(\mathbf{r}) = a_{+1}\mathbf{F}_{\pm,+1}(\mathbf{r})e^{i\varphi+i\beta z} + a_{-1}\mathbf{F}_{\pm,-1}(\mathbf{r})e^{-i\varphi-i\beta z}, \quad (46)$$

total Poynting vector and total optical spin current in the waveguide are given by the expressions

$$\langle P_z^{\text{in}}\rangle = (|a_{+1}|^2 - |a_{-1}|^2)\frac{c}{4a^2\pi^2}(n^2 + 3\chi^2 - 1),$$

$$\langle J_{zz}\rangle = (|a_{+1}|^2 - |a_{-1}|^2)\frac{c\chi}{4a^2\pi^2k_0}(n^2 + \chi^2). \quad (47)$$

One can see that when amplitudes of both waves are equal, there is no energy flux. This happens because two counter-propagating modes create a standing wave in the waveguide. However, optical spin current is non-zero for non-zero χ. Moreover, its direction and intensity is governed by the value of χ, which means that optical spin current is strictly positive for positive χ and strictly negative otherwise. And, the higher the value of χ, the higher the intensity of the optical spin current.

Indeed, both energy and optical spin current for such a superposition of an $m = 1$ and $m = -1$ modes with $a_{+1} = \cos\theta$ and $a_{-1} = \sin\theta$ is shown in Fig. 3, *b*. One can see that when amplitudes of both modes are equal, they form a standing wave. However, optical spin current is nonzero for any θ. Thus, it is possible to find such a regime, when energy flux is zero inside the waveguide, while optical spin current is not.

Conclusions

In this paper, we have shown that optical circular waveguide made of isotropic chiral material is a promising candidate for creating optical spin diodes and other opto spintronic devices with an asymmetric transfer characteristic. We have solved the eigenmode problem for such a waveguide and have shown that, by analogy with a circular dielectric waveguide, the fundamental mode of a circular chiral waveguide is the mode with an azimuthal number $m = \pm 1$. The main result of the paper are you the equations showing that the direction of the optical spin current in such waveguides is determined exclusively by the sign of the chirality parameter of the material from which the waveguide is made. Moreover, due to the symmetry of the system and the orthogonality of the waveguide modes, the chiral optical nanofiber supports configurations of standing electromagnetic waves with a non-zero optical spin current. We believe that our findings open new avenues for creating new energy efficient opto-spintronic devices for processing and transmitting information, which can serve as a good platform for further development of optical computing systems.

Supplementary Materials

We consider electromagnetic field in isotropic homogeneous chiral media. We start from Maxwell's equations

$$\begin{aligned} \nabla\times\mathbf{E} &= ik_0[\mu\mathbf{H} - i\chi\mathbf{E}],\\ \nabla\times\mathbf{H} &= -ik_0[\epsilon\mathbf{E} + i\chi\mathbf{H}],\\ \nabla\cdot[\epsilon\mathbf{E} + i\chi\mathbf{H}] &= 0,\\ \nabla\cdot[\mu\mathbf{H} - i\chi\mathbf{E}] &= 0. \end{aligned} \quad (48)$$

It is easy to show that the transversality of **E** and **H** fields still hold. From Eq. (48) it is possible to show that

$$\nabla\cdot[\epsilon\mu\mathbf{E} + i\chi\mu\mathbf{H} - i\chi\mu\mathbf{H} - \chi^2\mathbf{E}] = (\epsilon\mu - \chi^2)\nabla\cdot\mathbf{E} = 0,$$

and

$$(\epsilon\mu - \chi^2)\nabla\cdot\mathbf{H} = 0.$$

In chiral media, the basis of **E** and **H** fields is much less convenient than in usual dielectrics. We are looking for fields $\mathbf{F} = a\mathbf{E} + b\mathbf{H}$, and $\mathbf{G} = c\mathbf{E} + d\mathbf{H}$, such that

$$\nabla\times\mathbf{F} = ik_0\beta\mathbf{G}, \nabla\times\mathbf{G} = -ik_0\alpha\mathbf{F}. \quad (49)$$

Using Eqs. (48), and (49), we calculate

$$\nabla\times\mathbf{F} = \nabla\times[a\mathbf{E} + b\mathbf{H}] = ik_0[a(\mu\mathbf{H} - i\chi\mathbf{E}) + b(-\epsilon\mathbf{E} - i\chi\mathbf{H})] = = ik_0[(-ai\chi - b\epsilon)\mathbf{E} + (a\mu - bi\chi)\mathbf{H}), \quad (50)$$

$$\nabla\times\mathbf{G} = \nabla\times[c\mathbf{E} + d\mathbf{H}] = -ik_0[c(-\mu\mathbf{H} + i\chi\mathbf{E}) + d(\epsilon\mathbf{E} + i\chi\mathbf{H})] = = -ik_0[(ci\chi + d\epsilon)\mathbf{E} + (-c\mu + di\chi)\mathbf{H}). \quad (51)$$

Comparing Eqs. (50), and (51) equations with Eq. (49) results in the following system of equations.

$$\begin{bmatrix} -i\chi & -\epsilon & -\beta & 0 \\ \mu & -i\chi & 0 & -\beta \\ -\alpha & 0 & i\chi & \epsilon \\ 0 & -\alpha & -\mu & i\chi \end{bmatrix}\begin{bmatrix} a \\ b \\ c \\ d \end{bmatrix} = 0.$$

Solvability condition gives

$$\alpha\beta = (\sqrt{\epsilon\mu} \pm \chi)^2,$$

and coefficients are

$$b = \pm iaZ,\ c = \mp iaV,\ d = aZV,$$

$$Z = \sqrt{\frac{\mu}{\epsilon}},\ V = \sqrt{\frac{\alpha}{\beta}}.$$

Therefore

$$\begin{bmatrix} \mathbf{F} \\ \mathbf{G} \end{bmatrix} = \begin{bmatrix} 1 & \pm iZ \\ \mp iV & ZV \end{bmatrix}\begin{bmatrix} \mathbf{E} \\ \mathbf{H} \end{bmatrix}.$$

One can see that

$$\mathbf{G}_\pm = -iV\mathbf{F}_\pm.$$

Transition back to electric and magnetic fields is possible by the following transformation

$$\mathbf{E} = \frac{\mathbf{F}_+ + \mathbf{F}_-}{2},\ \mathbf{H} = \frac{\mathbf{F}_+ - \mathbf{F}_-}{2iZ}.$$

In such a basis, Maxwell equations become

$$\nabla\times\mathbf{F}_\pm = \pm k_0 n_\pm \mathbf{F}_\pm,\ n_\pm = n \pm \chi. \quad (52)$$

Such vectors are called Riemann-Silberstein vectors [25, 26]. We also note that from Eq. (52), $\nabla\times\mathbf{F}_\pm = 0$ automatically if $n_\pm \neq 0$.

Boundary conditions for electric and magnetic fields at the interface are $E_\tau^{\text{in}} = E_\tau^{\text{out}}$, $H_\tau^{\text{in}} = H_\tau^{\text{out}}$ where τ encodes tangential w.r.t interface component. One can derive boundary conditions for $\mathbf{F}_\pm$,

$$F_{+,\tau}^{\text{in}} + F_{-,\tau}^{\text{in}} = F_{+,\tau}^{\text{out}} + F_{-,\tau}^{\text{out}},\ \frac{F_{+,\tau}^{\text{in}} - F_{-,\tau}^{\text{in}}}{Z^{\text{in}}} = \frac{F_{+,\tau}^{\text{out}} - F_{-,\tau}^{\text{out}}}{Z^{\text{out}}}.$$

Time-averaged energy density in chiral media, in terms of Riemann-Silberstein vectors is

$$\langle W\rangle = \frac{\mathrm{Re}\{\mathbf{E}\cdot\mathbf{D}^*\} + \mathrm{Re}\{\mathbf{H}\cdot\mathbf{B}^*\}}{8\pi} =$$

$$= \frac{\mathrm{Re}\{\epsilon|\mathbf{E}|^2 + i\chi\mathbf{E}\cdot\mathbf{H}^*\} + \mathrm{Re}\{\mu|\mathbf{H}|^2 + i\chi\mathbf{H}\cdot\mathbf{E}^*\}}{8\pi} =$$

$$= \frac{\epsilon|\mathbf{E}|^2 + \mu|\mathbf{H}|^2 - \chi\mathrm{Im}\{\mathbf{E}\cdot\mathbf{H}^*\} - \chi\mathrm{Im}\{\mathbf{H}\cdot\mathbf{E}^*\}}{8\pi} =$$

$$= \frac{\epsilon|\mathbf{E}|^2 + \mu|\mathbf{H}|^2}{8\pi} = \frac{\epsilon}{32\pi}[|\mathbf{F}_+|^2 + |\mathbf{F}_-|^2].$$

Similarly, one can derive the time-averaged Poynting vector and the time-averaged optical spin current as

$$\langle\mathbf{S}\rangle = \frac{c}{8\pi}\mathrm{Re}\{\mathbf{E}\times\mathbf{H}^*\} = \frac{c}{32\pi Z}\mathrm{Re}\left\{\frac{(\mathbf{F}_+ + \mathbf{F}_-)\times(\mathbf{F}_+^* + \mathbf{F}_-^*)}{-i}\right\} =$$

$$= \frac{c}{32\pi Z}\mathrm{Im}\{\mathbf{F}_-\times\mathbf{F}_-^* - \mathbf{F}_+\times\mathbf{F}_+^*\}$$

and

$$\langle\hat{\mathrm{J}}_s\rangle = \frac{c}{16\pi\omega}\mathrm{Im}\{\hat{\mathbb{1}}\mathbf{E}\cdot\mathbf{H}^* - \mathbf{E}\otimes\mathbf{H}^* - \mathbf{H}^*\otimes\mathbf{E}\} =$$

$$= \frac{c}{64\pi\omega Z}\mathrm{Re}\{\hat{\mathbb{1}}(|\mathbf{F}_+|^2 - |\mathbf{F}_-|^2) - 2[\mathbf{F}_+\otimes\mathbf{F}_+^* - \mathbf{F}_-\otimes\mathbf{F}_-^*].$$

References

1. Li Y., Monticone F. Exploring the role of metamaterials in achieving advantage in optical computing. *Nature Computational Science*, 2024, vol. 4, no. 8, pp. 545–548. https://doi.org/10.1038/s43588-024-00657-w
2. McMahon P.L. The physics of optical computing. *Nature Reviews Physics*, 2023, vol. 5, no. 12, pp. 717–734. https://doi.org/10.1038/s42254-023-00645-5
3. Chanana A., Larocque H., Moreira R., Carolan J., Guha B., Melo E.G., et al. Ultra-low loss quantum photonic circuits integrated with single quantum emitters. *Nature Communications*, 2022, vol. 13, no. 1, pp. 7693. https://doi.org/10.1038/s41467-022-35332-z
4. Dong T., Liang J.J., Camayd-Muñoz S., Liu Y., Tang H., Kita S., et al. Ultra-low-loss on-chip zero-index materials. *Light: Science & Applications*, 2021, vol. 10, no. 1, pp. 10. https://doi.org/10.1038/s41377-020-00436-y
5. Blundell S., Radford T.W., Ajia I.A., Lawson D., Yan X.Z., Banakar M., et al. Ultracompact programmable silicon photonics using layers of low-loss phase-change material Sb_2Se_3 of increasing thickness. *ACS Photonics*, 2025, vol. 12, no. 3, pp. 1382–1391. https://doi.org/10.1021/acsphotonics.4c01789

Литература

1. Li Y., Monticone F. Exploring the role of metamaterials in achieving advantage in optical computing // Nature Computational Science. 2024. V. 4. N 8. P. 545–548. https://doi.org/10.1038/s43588-024-00657-w
2. McMahon P.L. The physics of optical computing // Nature Reviews Physics. 2023. V. 5. N 12. P. 717–734. https://doi.org/10.1038/s42254-023-00645-5
3. Chanana A., Larocque H., Moreira R., Carolan J., Guha B., Melo E.G., et al. Ultra-low loss quantum photonic circuits integrated with single quantum emitters // Nature Communications. 2022. V. 13. N 1. P. 7693. https://doi.org/10.1038/s41467-022-35332-z
4. Dong T., Liang J.J., Camayd-Muñoz S., Liu Y., Tang H., Kita S., et al. Ultra-low-loss on-chip zero-index materials // Light: Science & Applications. 2021. V. 10. N 1. P. 10. https://doi.org/10.1038/s41377-020-00436-y
5. Blundell S., Radford T.W., Ajia I.A., Lawson D., Yan X.Z., Banakar M., et al. Ultracompact programmable silicon photonics using layers of low-loss phase-change material Sb2Se3 of increasing thickness // ACS Photonics. 2025. V. 12. N 3. P. 1382–1391. https://doi.org/10.1021/acsphotonics.4c01789

6. Bader S.D., Parkin S.S.P. Spintronics. *Annual Review of Condensed Matter Physics*, 2010, vol. 1, pp. 71–88. https://doi.org/10.1146/annurev-conmatphys-070909-104123
7. Pulizzi F. Spintronics. *Nature Materials*, 2012, vol. 11, no. 5, pp. 367. https://doi.org/10.1038/nmat3327
8. Žutić I., Fabian J., Sarma S.D. Spintronics: Fundamentals and applications. *Reviews of Modern Physics*, 2004, vol. 76, no. 2, pp. 323–410. https://doi.org/10.1103/RevModPhys.76.323
9. Qin J., Sun B., Zhou G., Guo T., Chen Y., Ke C., et al. From spintronic memristors to quantum computing. *ACS Materials Letters*, 2023, vol. 5, no. 8. pp. 2197–2215. https://doi.org/10.1021/acsmaterialslett.3c00088
10. Yang H., Valenzuela S.O., Chshiev M., Couet S., Dieny B., Dlubak B., et al. Two-dimensional materials prospects for non-volatile spintronic memories. *Nature*, 2022, vol. 606, no. 7915, pp. 663–673. https://doi.org/10.1038/s41586-022-04768-0
11. Bliokh K.Y., Bekshaev A.Y., Nori F. Dual electromagnetism: helicity, spin, momentum and angular momentum. *New Journal of Physics*, 2013, vol. 15, pp. 033026. https://doi.org/10.1088/1367-2630/15/3/033026
12. Bliokh K.Y., Rodríguez-Fortuño F.J., Nori F., Zayats A.V. Spin–orbit interactions of light. *Nature Photonics*, 2015, vol. 9, no. 12, pp. 796–808. https://doi.org/10.1038/nphoton.2015.201
13. Bliokh K.Y., Nori F. Transverse and longitudinal angular momenta of light. *Physics Reports*, 2015, vol. 592, pp. 1–38. https://doi.org/10.1016/j.physrep.2015.06.003
14. Marrucci L., Manzo C., Paparo D. Optical spin-to-orbital angular momentum conversion in inhomogeneous anisotropic media. *Physical Review Letters*, 2006, vol. 96, no. 16, pp. 163905. https://doi.org/10.1103/PhysRevLett.96.163905
15. Erhard M., Fickler R., Krenn M., Zeilinger A. Twisted photons: new quantum perspectives in high dimensions. *Light: Science & Applications*, 2018, vol. 7, pp. 17146. https://doi.org/10.1038/lsa.2017.146
16. Nagali E., Giovannini D., Marrucci L., Slussarenko S., Santamato E., Sciarrino F. Experimental optimal cloning of four-dimensional quantum states of photons. *Physical Review Letters*, 2010, vol. 105, no. 7, pp. 073602. https://doi.org/10.1103/PhysRevLett.105.073602
17. Deriy I., Kornovan D., Petrov M., Bogdanov A. Optical spintronics: towards optical communication without energy transfer. *arXiv*, 2025, arXiv:2505.10489. https://doi.org/10.48550/arXiv.2505.10489
18. Wu X., Tong L. Optical microfibers and nanofibers. *Nanophotonics*, 2013, vol. 2, no. 5-6, pp. 407–428. https://doi.org/10.1515/nanoph-2013-0033
19. Nayak K.P., Kien F.L., Nakajima K., Miyazaki H.T., Sugimoto Y., Hakuta K. Nano-structured optical nanofibers for cavity-QED. *Proc. of the Conference on Lasers and Electro-Optics (CLEO)*, 2011, pp. QFC2. https://doi.org/10.1364/qels.2011.qfc2
20. Le Kien F., Rauschenbeutel A. Nanofiber-based all-optical switches. *Physical Review A*, 2016, vol. 93, no. 1, pp. 013849. https://doi.org/10.1103/PhysRevA.93.013849
21. Guo J., Liu X., Jiang N., Yetisen A., Yuk H., Yang C., et al. Highly stretchable, strain sensing hydrogel optical fibers. *Advanced Materials*, 2016, vol. 28, no. 46, pp. 10244–10249. https://doi.org/10.1002/adma.201603160
22. Russell P.S.J., Beravat R., Wong G.K.L. Helically twisted photonic crystal fibres. *Philosophical Transactions of the Royal Society A: Mathematical, Physical and Engineering Sciences*, 2017, vol. 375, no. 2087, pp. 20150440. https://doi.org/10.1098/rsta.2015.0440
23. Machnev A.A., Pushkarev A.P., Tonkaev P., Noskov R.E., Rusimova K.R., Mosley P.J., et al. Modifying light–matter interactions with perovskite nanocrystals inside antiresonant photonic crystal fiber. *Photonics Research*, 2021, vol. 9, no. 8, pp. 1462–1469. https://doi.org/10.1364/PRJ.422640
24. Kolchanov D.S., Machnev A., Blank A., Barhom H., Zhu L., Lin Q., et al. Thermo-optics of gilded hollow-core fibers. *Nanoscale*, 2024, vol. 16, no. 29, pp. 13945–13952. https://doi.org/10.1039/D3NR05310E
25. Bialynicki-Birula I., Bialynicka-Birula Z. The role of the Riemann–Silberstein vector in classical and quantum theories of electromagnetism. *Journal of Physics A: Mathematical and Theoretical*, 2013, vol. 46, no. 5, pp. 053001. https://doi.org/10.1088/1751-8113/46/5/053001
26. Belkovich I.V., Kogan B.L. Utilization of Riemann-Silberstein vectors in electromagnetics. *Progress in Electromagnetics Research B*, 2016, vol. 69, no. 1, pp. 103–116. https://doi.org/10.2528/pierb16051809

6. Bader S.D., Parkin S.S.P. Spintronics // Annual Review of Condensed Matter Physics. 2010. V. 1. P. 71–88. https://doi.org/10.1146/annurev-conmatphys-070909-104123
7. Pulizzi F. Spintronics // Nature Materials. 2012. V. 11. N 5. P. 367. https://doi.org/10.1038/nmat3327
8. Žutić I., Fabian J., Sarma S.D. Spintronics: Fundamentals and applications // Reviews of Modern Physics. 2004. V. 76. N 2. P. 323–410. https://doi.org/10.1103/RevModPhys.76.323
9. Qin J., Sun B., Zhou G., Guo T., Chen Y., Ke C., et al. From spintronic memristors to quantum computing // ACS Materials Letters. 2023. V. 5. N 8. P. 2197–2215. https://doi.org/10.1021/acsmaterialslett.3c00088
10. Yang H., Valenzuela S.O., Chshiev M., Couet S., Dieny B., Dlubak B., et al. Two-dimensional materials prospects for non-volatile spintronic memories // Nature. 2022. V. 606. N 7915. P. 663–673. https://doi.org/10.1038/s41586-022-04768-0
11. Bliokh K.Y., Bekshaev A.Y., Nori F. Dual electromagnetism: helicity, spin, momentum and angular momentum // New Journal of Physics. 2013. V. 15. P. 033026. https://doi.org/10.1088/1367-2630/15/3/033026
12. Bliokh K.Y., Rodríguez-Fortuño F.J., Nori F., Zayats A.V. Spin–orbit interactions of light // Nature Photonics. 2015. V. 9. N 12. P. 796–808. https://doi.org/10.1038/nphoton.2015.201
13. Bliokh K.Y., Nori F. Transverse and longitudinal angular momenta of light // Physics Reports. 2015. V. 592. P. 1–38. https://doi.org/10.1016/j.physrep.2015.06.003
14. Marrucci L., Manzo C., Paparo D. Optical spin-to-orbital angular momentum conversion in inhomogeneous anisotropic media // Physical Review Letters. 2006. V. 96. N 16. P. 163905. https://doi.org/10.1103/PhysRevLett.96.163905
15. Erhard M., Fickler R., Krenn M., Zeilinger A. Twisted photons: new quantum perspectives in high dimensions // Light: Science & Applications. 2018. V. 7. P. 17146. https://doi.org/10.1038/lsa.2017.146
16. Nagali E., Giovannini D., Marrucci L., Slussarenko S., Santamato E., Sciarrino F. Experimental optimal cloning of four-dimensional quantum states of photons // Physical Review Letters. 2010. V. 105. N 7. P. 073602. https://doi.org/10.1103/PhysRevLett.105.073602
17. Deriy I., Kornovan D., Petrov M., Bogdanov A. Optical spintronics: towards optical communication without energy transfer // arXiv. 2025. arXiv:2505.10489. https://doi.org/10.48550/arXiv.2505.10489
18. Wu X., Tong L. Optical microfibers and nanofibers // Nanophotonics. 2013. V. 2. N 5-6. P. 407–428. https://doi.org/10.1515/nanoph-2013-0033
19. Nayak K.P., Kien F.L., Nakajima K., Miyazaki H.T., Sugimoto Y., Hakuta K. Nano-structured optical nanofibers for cavity-QED // Proc. of the Conference on Lasers and Electro-Optics (CLEO). 2011. P. QFC2. https://doi.org/10.1364/qels.2011.qfc2
20. Le Kien F., Rauschenbeutel A. Nanofiber-based all-optical switches // Physical Review A. 2016. V. 93. N 1. P. 013849. https://doi.org/10.1103/PhysRevA.93.013849
21. Guo J., Liu X., Jiang N., Yetisen A., Yuk H., Yang C., et al. Highly stretchable, strain sensing hydrogel optical fibers // Advanced Materials. 2016. V. 28. N 46. P. 10244–10249. https://doi.org/10.1002/adma.201603160
22. Russell P.S.J., Beravat R., Wong G.K.L. Helically twisted photonic crystal fibres // Philosophical Transactions of the Royal Society A: Mathematical, Physical and Engineering Sciences. 2017. V. 375. N 2087. P. 20150440. https://doi.org/10.1098/rsta.2015.0440
23. Machnev A.A., Pushkarev A.P., Tonkaev P., Noskov R.E., Rusimova K.R., Mosley P.J., et al. Modifying light–matter interactions with perovskite nanocrystals inside antiresonant photonic crystal fiber // Photonics Research. 2021. V. 9. N 8. P. 1462–1469. https://doi.org/10.1364/PRJ.422640
24. Kolchanov D.S., Machnev A., Blank A., Barhom H., Zhu L., Lin Q., et al. Thermo-optics of gilded hollow-core fibers // Nanoscale. 2024. V. 16. N 29. P. 13945–13952. https://doi.org/10.1039/D3NR05310E
25. Bialynicki-Birula I., Bialynicka-Birula Z. The role of the Riemann–Silberstein vector in classical and quantum theories of electromagnetism // Journal of Physics A: Mathematical and Theoretical. 2013. V. 46. N 5. P. 053001. https://doi.org/10.1088/1751-8113/46/5/053001
26. Belkovich I.V., Kogan B.L. Utilization of Riemann-Silberstein vectors in electromagnetics // Progress in Electromagnetics Research B. 2016. V. 69. N 1. P. 103–116. https://doi.org/10.2528/pierb16051809
27. Snyder A.W., Love J. Optical Waveguide Theory. Chapman and Hall, 1983. 746 p.

27. Snyder A.W., Love J. *Optical Waveguide Theory*. Chapman and Hall, 1983, 746 p.
28. Seaborn J.B. *Hypergeometric Functions and Their Applications*. Springer, 2013, 268 p.

28. Seaborn J.B. Hypergeometric Functions and Their Applications. Springer, 2013. 268 p.

Authors

Ilya A. Deriy — Junior Researcher, Harbin Engineering University, Qingdao, 266000, China; Junior Reseacher, ITMO University, Saint Petersburg, 197101, Russian Federation, sc 57221052856, https://orcid.org/0000-0002-6515-9325, ilya.deriy@metalab.ifmo.ru

Danil F. Kornovan — PhD (Physics & Mathematics), Engineer, ITMO University, Saint Petersburg, 197101, Russian Federation, sc 56644703300, https://orcid.org/0000-0002-4851-0697, d.kornovan@metalab.ifmo.ru

Mihail I. Petrov — PhD (Physics & Mathematics), Associate Professor, Senior Researcher, ITMO University, Saint Petersburg, 197101, Russian Federation, Researcher ID K-5924-2012, https://orcid.org/0000-0001-8155-9778, m.petrov@metalab.ifmo.ru

Andrey A. Bogdanov — PhD (Physics & Mathematics), Senior Researcher, Harbin Engineering University, Qingdao, 266000, China; Senior Researcher, Associate Professor of Practice, ITMO University, Saint Petersburg, 197101, Russian Federation, sc 56393877900, https://orcid.org/0000-0002-8215-0445, a.bogdanov@metalab.ifmo.ru

Авторы

Дерий Илья Александрович — младший научный сотрудник, Харбинский Инженерный Университет, Циндао, 266000, Китай; младший научный сотрудник, Университет ИТМО, Санкт-Петербург, 197101, Российская Федерация, sc 57221052856, https://orcid.org/0000-0002-6515-9325, ilya.deriy@metalab.ifmo.ru

Корнован Данил Феодосьевич — кандидат физико-математических наук, инженер, Университет ИТМО, Санкт-Петербург, 197101, Российская Федерация, sc 56644703300, https://orcid.org/0000-0002-4851-0697, d.kornovan@metalab.ifmo.ru

Петров Михаил Игоревич — кандидат физико-математических наук, доцент, старший научный сотрудник, Университет ИТМО, Санкт-Петербург, 197101, Российская Федерация, Researcher ID K-5924-2012, https://orcid.org/0000-0001-8155-9778, m.petrov@metalab.ifmo.ru

Богданов Андрей Андреевич — кандидат физико-математических наук, старший научный сотрудник, Харбинский Инженерный Университет, Циндао, 266000, Китай; старший научный сотрудник, доцент практики, Университет ИТМО, Санкт-Петербург, 197101, Российская Федерация, sc 56393877900, https://orcid.org/0000-0002-8215-0445, a.bogdanov@metalab.ifmo.ru

Received 24.07.2025
Approved after reviewing 18.08.2025
Accepted 15.09.2025

Статья поступила в редакцию 24.07.2025
Одобрена после рецензирования 18.08.2025
Принята к печати 15.09.2025